ADVANCED ENGINEERING MATERIALS
www.aem-journal.com

Effect of High-Pressure Torsion on Hardness and Electrical Resistivity of Commercially Pure Cu

*Ajay Rijal, Shobhit P. Singh, Jae-Kyung Han, Megumi Kawasaki, and Praveen Kumar**

This manuscript is prepared on the occasion of the 80th birthday of Professor Terence G. Langdon and is dedicated to his impressive work in the general area of ultrafine-grained materials processed by severe plastic deformation

Commercially pure Cu is processed through high-pressure torsion (HPT) at 6 GPa up to 50 turns and stored under the ambient condition for 21 months. Subsequently, microhardness and electrical resistivity of the Cu samples are measured and correlated with the microstructure. Grain size monotonically decreases with the number of HPT turns and becomes saturated at ≈300 nm after an equivalent strain of ≈40. Considerable fractions of low-angle grain and twin boundaries are observed in the samples processed through HPT to low strains; however, their fractions decrease with increasing HPT turns. Consistently, although the hardness of the processed samples is greater than that of the annealed coarse-grained sample, it first decreases with HPT straining and subsequently increases to a saturated value of ≈160 HV. In contrast, the electrical resistivity of Cu first increases with HPT processing, then decreases and finally becomes saturated at a value of ≈22 nΩ m, which is slightly higher than the least value obtained in this study. The obtained results are compared with the literature on HPT processing of Cu, and the usefulness of the ambient ageing for optimizing the hardness-conductivity relationship is discussed.

1. Introduction

It is now well-established that severe plastic deformation (SPD) has extraordinary ability to produce metallic materials having ultrafine grains and an excellent combination of mechanical properties.[1–4] Among all the SPD processes, equal-channel angular pressing (ECAP), wherein a billet is pushed through a die with an angular channel with a bent angle, ϕ, of as low as 90°,[5] and high-pressure torsion (HPT), which enables imposing severe torsional strains into a disk-shaped sample by placing it in between two anvils and rotating one of the anvils while applying a very large uniaxial compressive stress,[6] are the most extensively used techniques, primarily due to ease of their processing procedure and their effectiveness in imposing very large strains into samples without cracking or fracture. Majority of the work performed in general area of SPD have also focused on these two SPD processes.

Compared with the ECAP and other SPD processes, HPT can impose very high strains (e.g., ≈1000) and hence can produce true nanoscale grains with a larger fraction of high-angle boundaries in significantly shorter processing time.[7] Such an ability of HPT makes it suitable for quickly studying the effect of extreme strains on structure–property relationship relevant for an application. In addition, unlike ECAP that applies uniform strain throughout the sample, the strain imposed on a sample during HPT varies gradually with the distance from the center of the disk to its periphery, r, as per the following equation[8]

$$\varepsilon_{eq} = \frac{2}{\sqrt{3}} \frac{\pi r N}{h} \tag{1}$$

where ε_{eq} is the equivalent von Mises strain at a point at r, N is the number of turns, and h is the thickness of the sample. Hence, HPT processing allows to study effect of large plastic strain on the microstructure as well as the physical properties, through local probing, using only one sample. This may help to perform high-throughput experiments and material combinatorics. Hence, studying effects of gradient straining on multiple properties of a material processed by HPT is quite attractive, and it is evident from increasing popularity of HPT in the last two decades. Herein, microstructure and various mechanical properties, such as hardness,[9,10] fatigue,[11–13] wear,[14–17] etc., of various metals and alloys processed through HPT have been well studied; however, only a few reports have discussed the effect of HPT processing on electrical conductivity (or resistivity) of materials.[18–22] It is particularly interesting that the ultrafine

A. Rijal, S. P. Singh, Dr. P. Kumar
Department of Materials Engineering
Indian Institute of Science
Bangalore 560012, India
E-mail: praveenk@iisc.ac.in

J.-K. Han, Dr. M. Kawasaki
School of Mechanical
Industrial and Manufacturing Engineering
Oregon State University
Corvallis, OR 97731, USA

The ORCID identification number(s) for the author(s) of this article can be found under https://doi.org/10.1002/adem.201900547.

DOI: 10.1002/adem.201900547

grains leading to high strength as per the Hall–Petch relation[23,24] may also enhance the overall electron scattering at the grain boundaries of SPD-processed metals. This can potentially reduce the electrical conductivity[25] of HPT-processed metals. Hence, it is a major challenge to increase the strength of a material without hampering its conductivity. Accordingly, exploration of potentially meeting this challenge through HPT processing, i.e., extreme straining, is the main goal of this work.

Cu is an interesting metal for exploring techniques suitable for meeting the aforementioned challenge, as it is one of the most popular metals used in the electrical connectors and circuits, due to its excellent electrical conductivity; however, it does not have very high strength.[18] It should be noted that high strength (or hardness) is warranted especially for connector applications, such as in button connectors, alligator clips, etc. If the size of these connectors is small (e.g., <10 mm), then these can be readily fabricated from the HPT-processed disks or ECAP-processed bars and billets. However, it should be ensured that the electrical conductivity of Cu should not only remain high (i.e., as close to the annealed state as possible) but should also not deteriorate during service (i.e., equivalently, during room temperature ageing). Nevertheless, a limited number of reports have focused on the above challenge of obtaining high hardness, high conductivity in Cu processed by HPT.[18–20]

Accordingly, the present report evaluates the effect of HPT on the hardness and the electrical resistivity (or conductivity) of commercially pure (CP) Cu, which is a better contender to be used in connectors as compared with high-purity Cu, due to its inherent higher strength and better microstructural stability. The CP Cu disks were processed to very high HPT turns (of 50) and stored under ambient condition for 21 months. Hardness as well as electrical resistivity of these samples was measured as a function of the distance from the disk center to determine the HPT strain-property variations. In addition, a detailed analysis of microstructure was performed to gain important insights into processing–structure–property relationships. This report demonstrates the feasibility of using HPT for enhancing the hardness of CP Cu without significantly affecting its electrical conductivity.

2. Experimental Section

A commercially pure electrical grade Cu was selected as the material in this study. Disks of 10 mm diameter and 1 mm thickness were machined, which were then isothermally annealed at 600 °C for 1 h for homogenizing the microstructure and removing residual stresses induced due to the machining. The disks were then thinned to a final thickness of 0.85 mm. Subsequently, HPT processing was performed using a quasi-constrained HPT facility at room temperature by applying a pressure of 6 GPa for ½, 10, and 50 turns at 1 rpm. The as-annealed and the HPT-processed samples were stored under ambient conditions for 21 months.

Hardness of the samples was measured using a Vickers microhardness tester with a pyramid-shaped diamond indenter. Prior to the microhardness measurements, one of the flat surfaces of samples was metallographically polished up to 50 nm surface finish using colloidal silica. Vickers microhardness testing was performed by applying a load of 100 g onto the polished samples for 15 s. Numerous indentations were made onto a sample along two perpendicular diameters in a fashion schematically illustrated in **Figure 1**. As shown in Figure 1, for the collection of the data at a point, five measurements were taken at and around the point, respectively. Each indent was separated by a distance of 2.5 times the diagonal of the indent from the nearest indents to avoid any effect of cold work from the previous indentation. Hence, as per the schematic shown in Figure 1, a total of 20 indents was made for a given magnitude of the radial distance (or equivalently a strain—see Equation (1)). The results of all these 20 measurements were averaged to calculate the representative hardness values as a function of r, thus an equivalent strain imposed by HPT (except $r = 0$). In this study, this average hardness value will be reported along with an error bar showing the standard deviation of all datum points used to calculate the average hardness. One may refer to an earlier study[26] for the details of the aforementioned procedure for measuring hardness.

For measurements of electrical resistivity, the Cu disk samples were firstly mounted in a polymer resin and then metallographically polished up to 50 nm surface finish using colloidal silica. At the end of this process, the thickness of the samples was reduced to 0.5 mm. A thin strip of ≈1 mm width and 10 mm length along with one of the diameters of the sample was cut from each resin-mounted sample using a low-speed diamond saw. This strip was again sliced into five pieces of equal lengths. Then, the sliced pieces were removed from polymer resin by dissolving the later in acetone. Electrical resistivity of these miniaturized coupons was measured using a customized setup, as schematically illustrated in **Figure 2**a, as per four probe method. As shown in

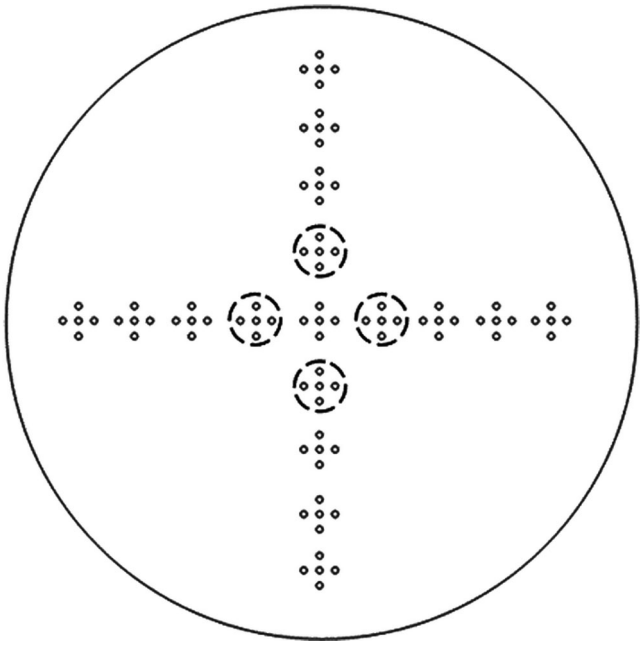

Figure 1. A schematic illustration showing the procedure followed in this study for performing microhardness tests using Vickers hardness tester. For illustration purpose, a group of five points corresponding to a point in the radial direction is inscribed by circles with dashed boundary. The radial distances of the representative points were 0, ±1, ±2, ±3, and ±4 mm away from the center of the disk, along each diameter.

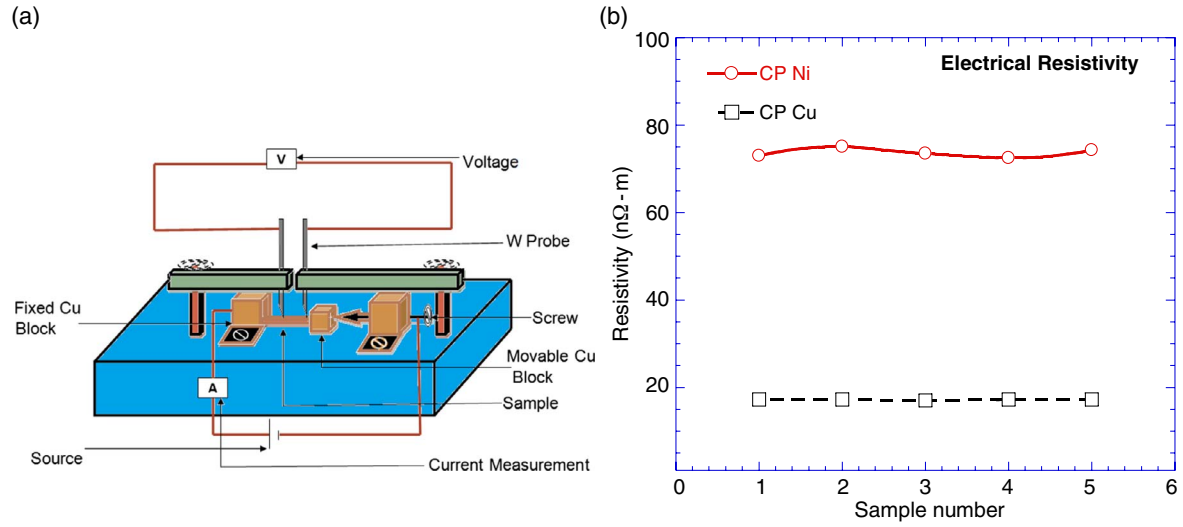

Figure 2. a) A schematic illustration of the test setup used for measuring the electrical resistivity of samples in this study, and b) validation of the accuracy of the measurement of resistivity using the setup shown in (a) by testing two commercially pure metals, whose electrical resistivity values were known.

Figure 2a, firstly a sample was placed in between two high-purity Cu blocks, which were then pushed onto the sample with the help of a screw attached to one of the Cu blocks (i.e., movable Cu block). The screw and the fixed Cu block were connected to an external high-precision power supply. As shown in Figure 2a, voltage drop between two points along the length of the sample was measured using two thin W electrodes, which were fixed on the outer sliders with the support of small screws. Once the electrodes were carefully placed on the top surface of the metallographically polished samples, they were connected to a nanovoltmeter for measuring the voltage drop with a resolution of 10 nV. These fine W electrodes were fabricated from a W rod of 1 mm diameter by grinding and, subsequently, chemically etching in hydrofluoric acid (HF), and had a tip diameter of 50 μm. Since W has high stiffness and hardness, it could easily make a small indent into the top surface of the CP Cu samples, thereby enabling accurate measurements of the distance between the two points on the sample across which the voltage drop was measured, l, using an optical microscope. The distance between these two points was kept close to 1 mm.

Once the hardware setup was completed, an electric current ranging from 0.1 to 0.9 A was passed through the sample, and the corresponding voltage drop was measured. The voltage drop was plotted as a function of the applied current and the best-fit line was drawn, whose slope was taken as the value of resistance of the sample, R, between the two points over which the voltage drop was measured. Subsequently, resistivity of the sample, ρ, was calculated using the following relation

$$\rho = \frac{RA}{l} \tag{2}$$

where A is the cross-sectional area of the samples (through which a current of uniform density was passed). Validation of the aforementioned test setup and procedure was performed by measuring and comparing the electrical resistivity, measured along several directions, of coarse-grained CP Cu and CP Ni having the same dimensions as of the actual samples (i.e., $2 \times 1 \times 0.5$ mm^3). The results are shown in Figure 2b where the resistivity values of the CP Cu and CP Ni were measured as 17.3 ± 0.3 and 73.0 ± 3.0 nΩ m, respectively, which were very close to their respective standard values of 17.2[27] and 75.0 nΩ m,[28] respectively.

Microstructural analysis was performed using electron backscatter diffraction (EBSD) on the metallographically polished Cu samples before and after processing by HPT. For EBSD, the metallographically polished samples were further electropolished using the standard D-2 electrolyte solution, which is prepared by mixing 40% phosphoric acid, 25% ethanol, 5% propan-1-ol, 29% water, and 1% urea.[29] The Cu sample, which was connected to the cathode, and the steel anode were dipped into the electrolyte, which was constantly agitated using a magnetic stirrer and was maintained at 5 °C. An optimized combination of voltage and current of 25 V and 0.7 A, respectively, was applied for 10 s to obtain a mirror finished surface required for the EBSD analysis. EBSD analysis was conducted at different regions of the disk samples to evaluate the effect of HPT strain on the microstructure and crystallographic texture. For the EBSD analysis, a step size of 50 nm was used for ultrafine grains, whereas a step size of 1 μm was used for the coarse-grained sample (i.e., unprocessed sample). Any misorientation exceeding 1° was considered as a boundary to quantify the grain size, whereas a misorientation angle of 15° was used to distinguish between a high-angle boundary and a low-angle boundary. Grain sizes of the materials were measured by a mean linear intercept method using OIM software.

3. Results

3.1. Effect of HPT on Microhardness

Figure 3a shows the variation of the hardness as a function of the distance from the center of the CP Cu disks after annealing

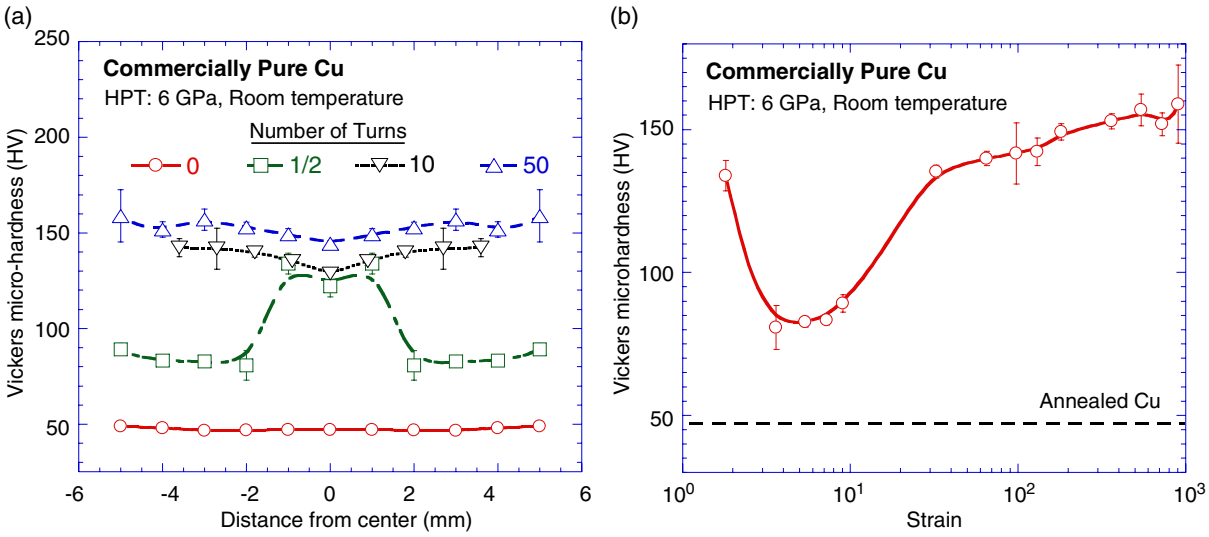

Figure 3. Variation of microhardness of CP Cu as function of a) radial distance away from the center and b) the effective strain imposed during HPT processing. The hardness profile in (a) was radially symmetric and each datum points here corresponds to ten readings, whereas each datum point in (b) corresponds to 20 measurements. It should be noted that, throughout this manuscript, the mentioned equivalent strain is solely due to the HPT processing.

without HPT (0 turn) and after HPT for ½, 10, and 50 turns followed by 21 months of storage under ambient conditions or ambient-ageing. As shown in Figure 3a, the hardness of the coarse-grained Cu, i.e., without HPT, was the minimum, equal to ≈47 HV with a little variation across the sample, of all the samples. Figure 3a also shows that the hardness of CP Cu samples monotonically increased with HPT processing; however, the difference between the samples processed through 10 and 50 turns was marginal. The hardness at the center of the sample processed to ten turns of HPT was ≈130 HV, which then gradually increased to 140 HV near its periphery. In contrast, the hardness of CP Cu increased to ≈155 HV throughout the sample after 50 turns of HPT. This confirms homogenization of the microstructure throughout 10 mm diameter disks once a certain strain was imposed through HPT. Similar trend was observed in other face-centered cubic (FCC) metals, where the hardness of materials showed a saturation in the value after large number of HPT turns.[9,30–32] However, the hardness profile of Cu sample processed to ½ turn of HPT followed by ambient-ageing was noticeably nonuniform. In practice, the value of microhardness in the center was ≈120 HV, which gradually increased to a value of ≈135 HV at a distance of 1 mm from the center; notwithstanding, the hardness sharply dropped to a value of only ≈80 HV at a distance of 2 mm from the center before finally attaining a value of ≈90 HV near the periphery of the sample. Such a variation in ½ turn data is actually consistent with the literature on HPT processed–ambient aged Cu,[33,34] whereas it is quite different than the hardness variation of CP Cu immediately after HPT.[33] A detailed discussion on the structure-property relationship responsible for such a contrasting behavior will be provided in Section 4.1.

Figure 3b shows the variation of hardness of CP Cu as a function of the equivalent strain imposed by HPT, as given by Equation (1). For the ease of representation of the data, the strain in Figure 3b is shown on a log-axis and hence the hardness data of the coarse-grained sample without HPT (i.e., $\varepsilon_{eq} = 0$) is shown by a horizontal broken line at ≈47 HV in the plot. Figure 3b shows that the hardness of the CP Cu increased to ≈135 HV at the onset of the HPT processing (i.e., $\varepsilon_{eq} = 1.8$), followed by a rapid decrease to a value of only ≈80 HV at an equivalent strain of 3.6. Thereafter, the hardness value increased rapidly up to a value of 135 HV and gradually increased to a value of ≈160 after a strain of ≈900. The sharp hardness drop followed by a rapid increase in the very early stage of torsional straining becomes apparent in the semi-log plot, whereas a conventional display of the hardness changes in a linear–linear graph fails to discern such hardness change in an earlier stage of the plastic deformation in the Cu samples.

3.2. Effect of HPT on Electrical Resistivity

Figure 4 shows the variation of electrical resistivity as function of equivalent strain for the CP Cu after HPT followed by ambient ageing. The material in an annealed condition without processing showed an electric resistivity of 17.3 nΩ m, as shown by a horizontal broken line, and the results from references[18–20] are included in the plot for comparison purposes. The electrical resistivity of the CP Cu increased to 21.0 nΩ m after a small strain of ≈7, followed by a drop to a value of 17.6 nΩ-m. This drop was followed by a gradual increase in the resistance to a value of ≈22.0 nΩ m for a strain of ≈400, finally decreasing to a value of 19.5 at the strain of ≈680. These changes are more than the error bar associated with these measurements, and hence, the effect of HPT processing on the nonmonotonous fluctuation of electrical resistivity should be considered for the CP Cu processed through HPT followed by ambient-ageing.

The variation and overall values of electrical resistivity obtained in this study are similar to that reported on high-purity Cu by Edalati et al.,[18] where they performed HPT processing at 2 GPa and measured average resistivity of 4 mm long sample as compared with ≈1 mm long sample in this study. However,

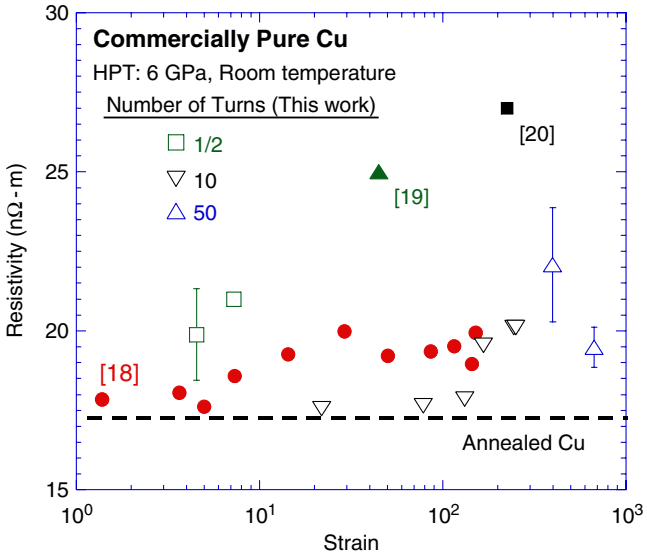

Figure 4. Variation of the electrical resistivity of HPT processed CP Cu as function of the strain imposed during HPT. The datum points reported by Edalati et al.,[18] who performed HPT for ¼ to 20 turns by applying a pressure of 2 GPa on high-purity Cu, Zhilyaev et al.,[19] who performed HPT for five turns by applying a pressure of 6 GPa on CP Cu and Zhilyaev et al.,[20] who performed HPT for five turns by applying a pressure of 6 GPa on the machined chips of CP Cu are also plotted as filled circles, upright triangle and square, respectively, in the above graph for the ease of comparison with the results obtained in this study.

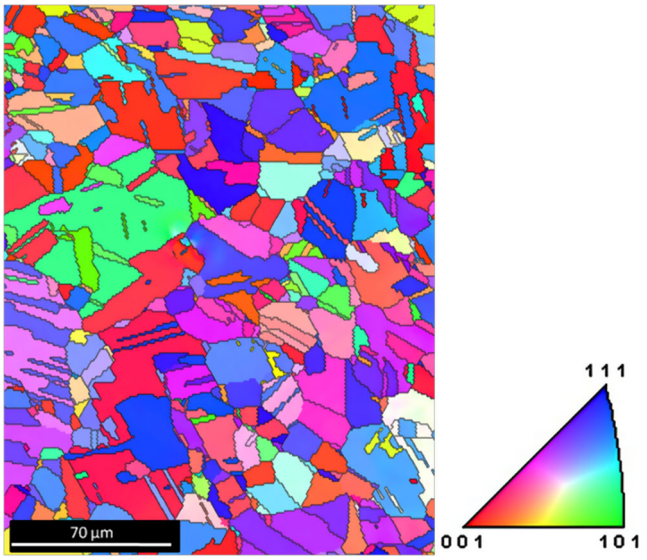

Figure 5. IPF map of annealed coarse-grained Cu, showing the grain structure and the distribution of crystallographic orientations. The legend on the right show the color map for IPF.

the electrical resistivity of CP Cu was only marginally affected by the HPT processing (e.g., within ±10% over a strain of 900—as shown in Figure 4). Hence, the effects of HPT pressure, purity of Cu, and microstructural inhomogeneity do not affect the electrical resistivity of HPT-processed Cu. In contrast, Zhilyaev et al.[20] observed a maximum value of ≈27.0 nΩ m for the electrical resistivity of the HPT-consolidated machined chips of CP Cu, which is significantly higher than the resistivity values obtained in this study. Here, HPT consolidation was performed at 6 GPa for 5 turns. Moreover, Zhilyaev et al.[19] also reported a high value of electrical resistivity of ≈25.0 nΩ m for CP Cu samples processed at 6 GPa to five turns of HPT.

3.3. Microstructural Characterization

Figure 5 shows a representative inverse pole figure (IPF) of the annealed coarse-grained Cu before HPT, suggesting that the crystallographic texture of the annealed sample was fairly random. Although the fraction of (101)-orientated grains in this particular IPF map was lesser than other major orientations, examination of other IPF maps did not show dominance of any one particular crystallographic texture. The grain size of the annealed Cu was measured as ≈11 μm. It also shows the presence of annealing twins in the annealed Cu samples. The total length of the twins per unit area, thus twin density, was $\approx 1.8 \times 10^{-1}\ \mu m^{-1}$.

Figure 6a–d shows a series of IPF maps taken at locations of $r = 0.6$, 2.0, 3.2, and 4.2 mm, respectively, for the CP Cu sample processed for ½ turn of HPT followed by ambient ageing. A careful observation of Figure 6 shows that the average grain size, d, did not change monotonically with increasing r. In practice, an average grain size of ≈1.5 μm at $r = 0.6$ mm increased to ≈2.5 μm at $r = 2.0$ mm and then gradually decreased to ≈1.5 μm near the periphery at $r = 4.2$ mm of the Cu disk. Similarly, twin density of $8.3 \times 10^{-1}\ \mu m^{-1}$ at $r = 0.6$ mm decreased to $7.0 \times 10^{-1}\ \mu m^{-1}$ at $r = 2.0$ mm and to $\approx 6.4 \times 10^{-1}\ \mu m^{-1}$ at $r = 4.2$ mm. Nevertheless, the increased twin density in comparison with that before HPT involves formation of the deformation twins in the HPT-processed CP Cu. Furthermore, the total length per unit area of the low and high angle grain boundaries changed from 2.47 and $2.24\ \mu m^{-1}$, respectively, at $r = 0.6$ mm to 0.75 and $2.02\ \mu m^{-1}$, respectively, at $r = 0.6$ mm in the CP Cu disk following HPT.

The nonmonotonous variation in the grain size can explain the nonuniform hardness profile for the Cu sample after HPT for ½ turn as shown in Figure 3a. In practice, the grain size in the central region was the smallest leading to the highest hardness in the sample as per Hall–Petch relationship. On the contrary, the grains near the disk periphery were only marginally (≈4.8%) larger than the grains in the central regions, but the hardness at the peripheral region was substantially lower than that of the central region after ½ turn. This anomalous deviation from Hall–Petch relation may be attributed to the significant decrease in the total length of the twin and the low-angle grain boundaries in the peripheral region as compared with the central region. It should be noted that the difference in the total length of high-angle grain boundaries in between these two regions was relatively less significant. Hence, although grain size is an important contributor to the strengthening of CP Cu, the role of boundaries (e.g., twin and low- and high-angle grain boundaries) is critical in determining the overall strength of the sample. This will be further discussed in Section 4.1.

Figure 7 shows the IPF maps taken at (a) 1.0, (b) 3.0, and (c) 4.2 mm away from the disk center after HPT for ten turns

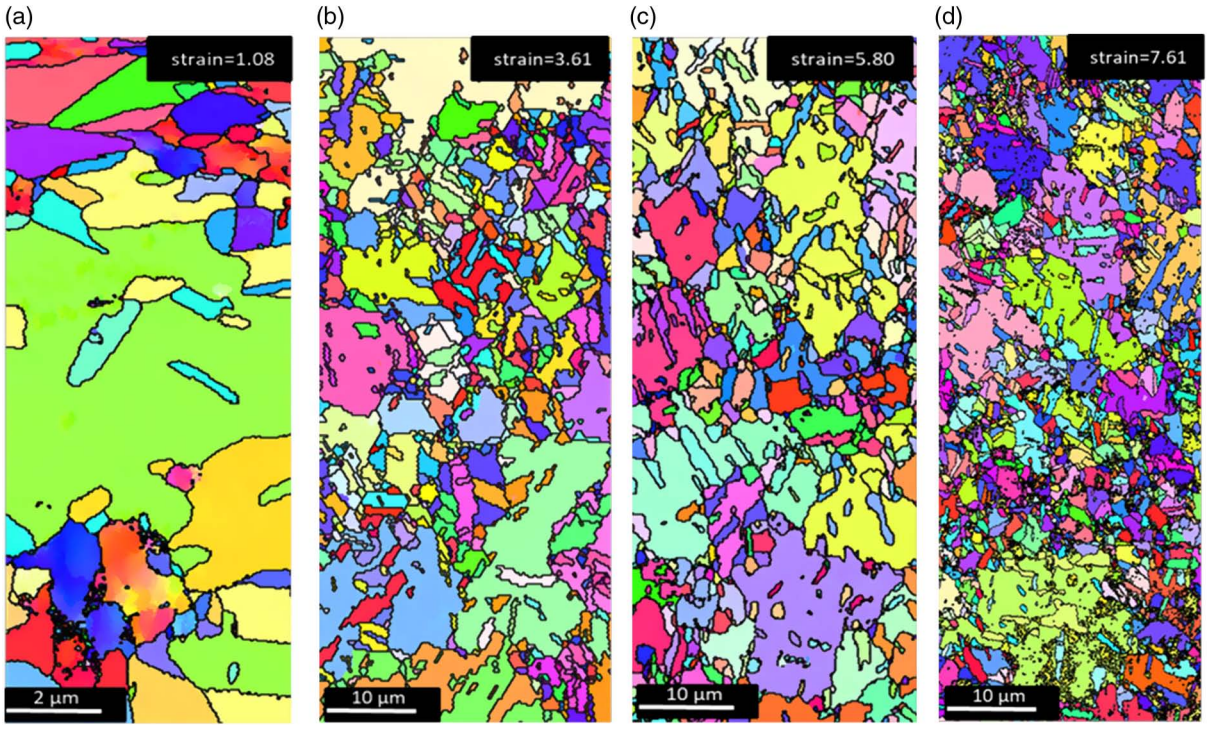

Figure 6. IPF maps of CP Cu disks processed up to ½ turn of HPT at various distances away from the center of the disk: a) 0.6, b) 2, c) 3.2, and d) 4.2 mm. The corresponding average strain value is shown in the top-right corner of each IPF map. The color-coded legend for IPF maps is shown in Figure 5.

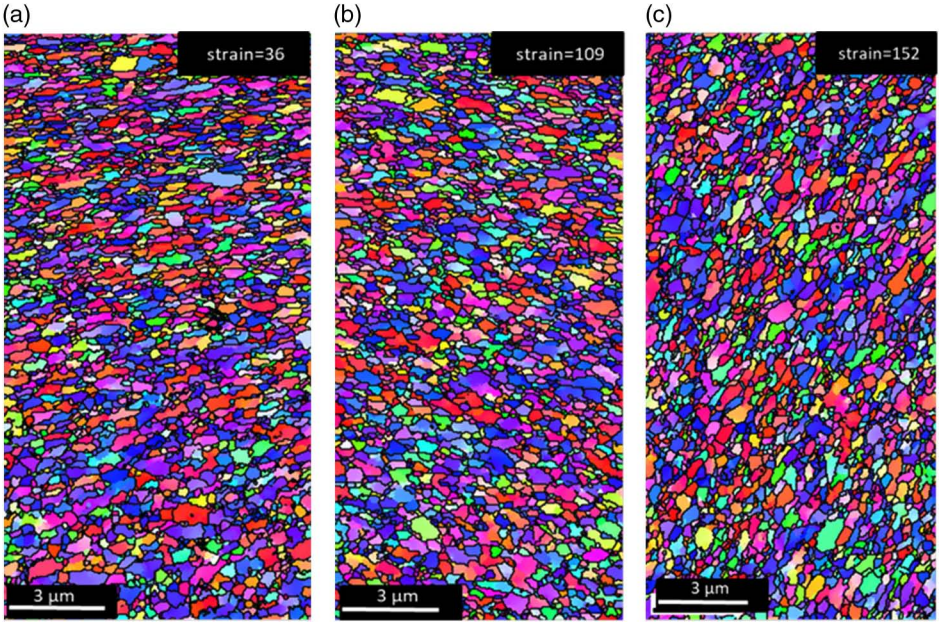

Figure 7. IPF maps showing various locations in the CP Cu disk processed up to ten turns of HPT: The average radial distance of each location was a) 1, b) 3, and c) 4.2 mm from the center. The corresponding average strain value is shown in the top-right corner of each IPF map. The color-coded legend for IPF maps is shown in Figure 5.

and **Figure 8** shows the IPF maps taken at (a) ≈0.1, (b) 4, and (c) 4.5 mm from the disk center after 50 turns of HPT. A comparison of Figure 7a–c and 8a–c shows an insignificant change in the size and morphology of grains with the distance from the centers of the CP Cu disks processed through ≥10 turns by HPT. Furthermore, unlike the annealed and the ½ turn HPT

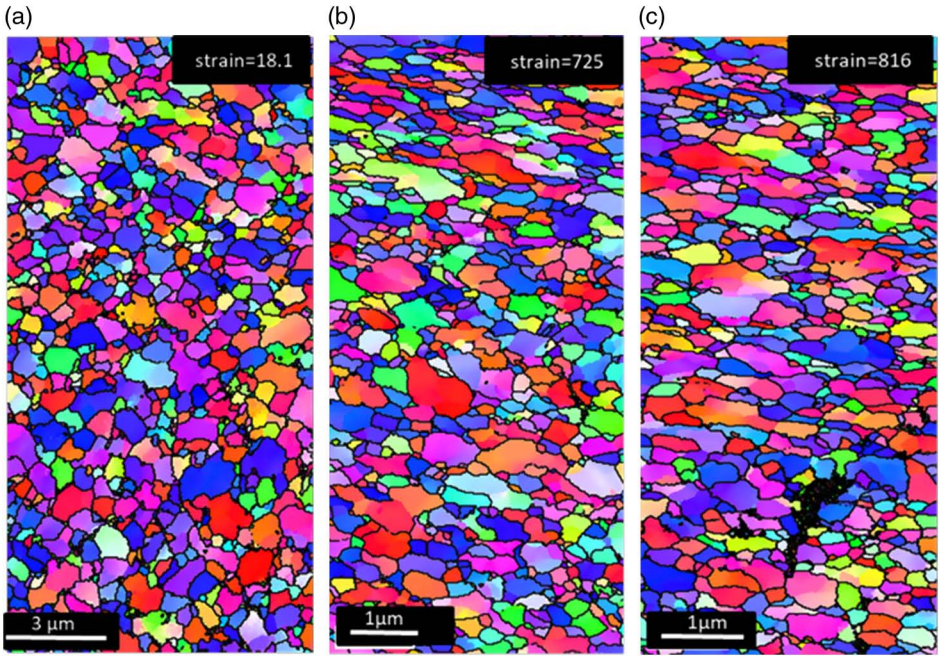

Figure 8. IPF maps showing various locations in the CP Cu disk processed up to 50 turns of HPT: The average radial distance of each location was a) ≈0.1, b) 4, and c) 4.5 mm from the center. The corresponding average strain value is shown in the top-right corner of each IPF map. The color-coded legend for IPF maps is shown in Figure 5.

samples, these samples had significantly fewer twins. Moreover, as shown from a comparison of Figure 8a–c (and also 7a–c), the morphology of grains in the locations away from the central regions was slightly elongated; this may be attributed to the rotational shear associated with the HPT processing. Overall, these CP Cu disks after HPT for 10 and 50 turns demonstrated random crystallographic texture.

Figure 9 summarizes the EBSD data shown in Figure 6–8 by plotting the variations of grain size (d), length per unit area of the low-angle grain boundaries (l_{LAGB}) and the high angle grain boundaries (l_{HAGB}), and length per unit area of the total grain boundaries (l_{TGB}) and length per unit area of the twin boundaries, thus twin density (l_{TB}) as a function of the equivalent strain imposed during HPT processing. As shown in Figure 9a, the refined grain size of 1.5 μm increased slightly to 2.5 μm at the onset of HPT straining and rapidly decreased to a saturated value of ≈300 nm after the HPT strain of ≈40. This is consistent with other studies showing the measured grain sizes of a few hundred nanometers in Cu by HPT processing.[18–20] The value of l_{LAGB} decreased monotonically up to a strain of 3 and remained low up to a strain of 5; thereafter, it increased to saturate with the HPT processing. The drop of l_{LAGB} at strain of <5 is attributed to the formation of subgrains due to the plastic deformation, which then transform into grains with high-angle grain boundaries upon continued plastic deformation by HPT. A comparison of Figures 9b,c shows that even after l_{LAGB} saturates its upper limit, the overall length of the high angle grain boundaries was more than the low-angle grain boundaries, and the difference tends to be apparent with increasing numbers of HPT turns through 10 to 50 turns. Hence, as shown in Figure 9d, the variation of l_{TGB} followed the trend of l_{HAGB}. Finally, as shown in Figure 9e and discussed in context of Figure 7 and 8, the overall length of the twin boundaries decreased drastically with continued HPT processing. Although a slight increase in the twin boundaries was noted at very high strain, it is reasonable to assume that a saturation in the total length of twin boundaries occurred at a comparatively low value of strain of ≈40. A comparison of Figure 9d,e shows that the length of twin boundaries was comparable with the length of the grain boundaries only at small strains, and hence, the contribution of twins in obstructing dislocations (i.e., slip) or scattering electrons will be significant in the CP Cu samples processed for low number of HPT turns.

4. Discussion

4.1. Hardness: Structure–Property Relationship

Figure 10a shows the variation of hardness as a function of the inverse of square root of grain size, d, for the CP Cu samples processed by HPT. A linear variation between the hardness and $d^{-0.5}$ is delineated by a dark dashed line for most of the datum points, and the result clearly shows the validity of the Hall–Petch relationship for the HPT-processed CP Cu samples. The main outlier, which is shown by an arrow in Figure 10a, was obtained from the central region of the disk processed for ½ turn by HPT. As discussed earlier, the grains in the central region of the sample were relatively very small and comprised of significantly large numbers of twins as compared with the grains in the regions away from the center. Since twin boundaries provide an additional resistance against glide of dislocation,[35] the presence of twins effectively reduces the grain size that one should use in the Hall–Petch relationship. In other words, the datum

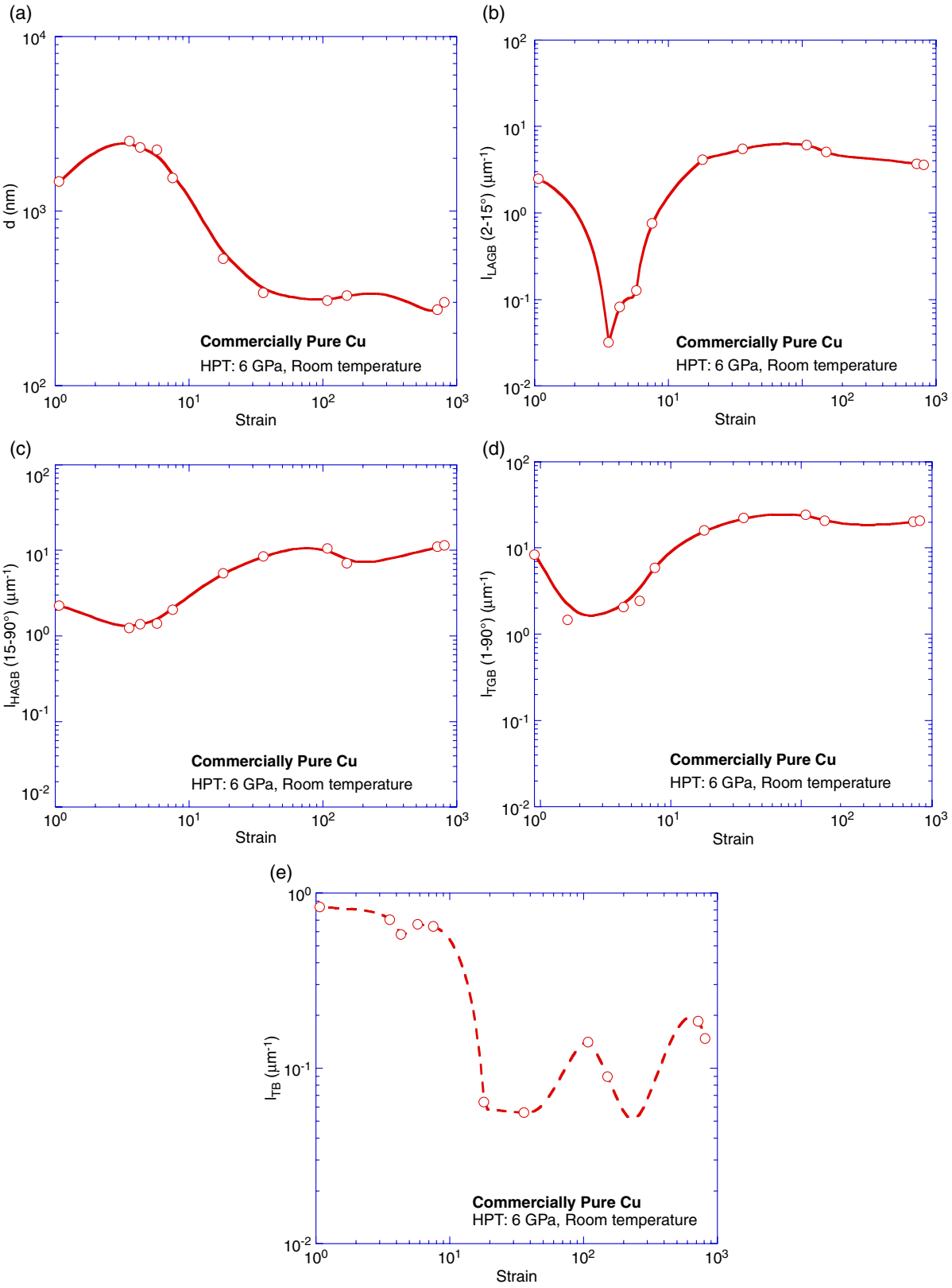

Figure 9. Variation of a) grain size (d) and length per unit area of the b) low-angle boundaries (l_{LAGB}), c) high-angle boundaries (l_{HAGB}), d) total grain boundaries (l_{TGB}), and e) twin boundary (l_{TB}) as a function of strain imposed during HPT processing. Here, the data for coarse-grained CP Cu are not shown.

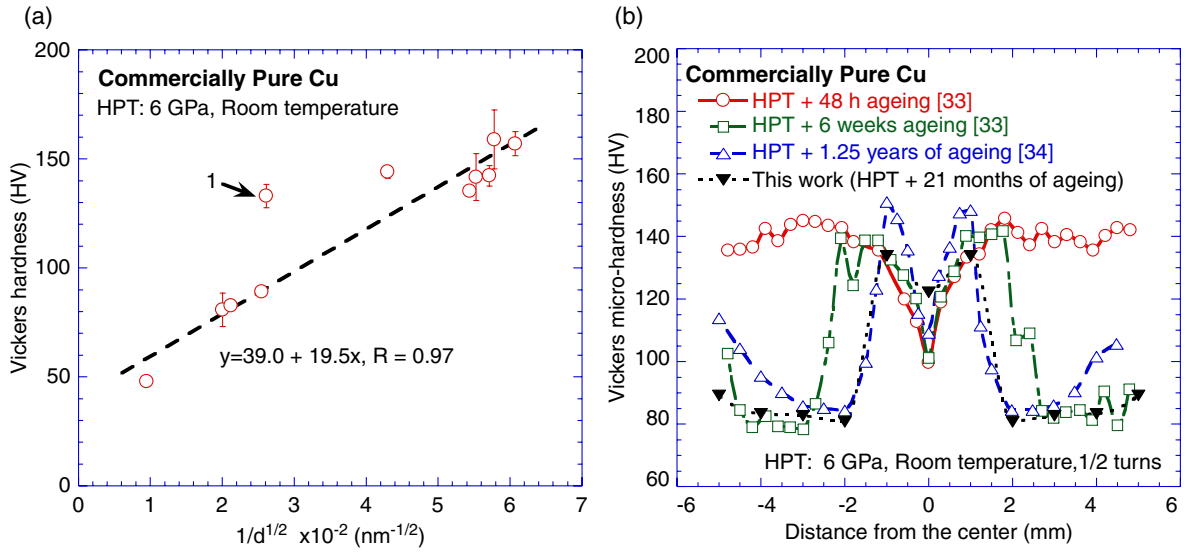

Figure 10. a) Variation of Vickers hardness as function of the inverse of the square root of the grain size. The dashed line shows the best linear fit passing through all datum points except for the point shown by the arrow. The corresponding equation, along with the regression parameter for the curve fitting, R, is shown next to the line. Point 1 was in the CP Cu disk processed through ½ turn of HPT at a distance of 0.6 mm away from the center. b) Variation of the hardness as function of distance from the center of the CP–Cu disk processed through ½ turn of HPT. Previously reported data are also plotted for comparison and highlighting the effect of ambient-ageing on hardness of the CP Cu samples processed through HPT.

point would shift toward its right, and hence, it would come closer to the dashed Hall–Petch line in Figure 10a, if an effective grain size could account for twins. Thus, the grain refinement and the hardness increase were correlated by applying the Hall–Petch relationship for the CP Cu in an as-annealed condition without HPT and after HPT through 50 turns at the center and edge positions.

As discussed in context of Figure 6, the grain size at the off-center in the central region was significantly smaller than that in the peripheral region of the CP Cu disk after ½ turn HPT followed by ambient ageing. Such a variation is possible at the locations that has accumulated more strain during HPT if grains have recovered and recrystallized during the ambient-ageing. In practice, this has been reported earlier for an HPT-processed high-purity Cu by Edalati et al.[36] and an HPT-processed CP Cu by Langdon and coworkers.[37] Figure 10b shows the data reported in references,[33,34] along with the results obtained in this study, on CP Cu disks processed by HPT for ½ turn. As shown in Figure 10b, the hardness profile of the CP Cu disk after 48 h of the HPT processing showed the general behavior with strain hardening, wherein more strained peripheral regions showed higher hardness as compared with the central region. However, the hardness profile drastically evolved as the HPT-processed sample was ambient-aged for 6 weeks, marked by a significant decrease in the hardness of the peripheral regions. With further ambient-ageing, the region of the high hardness continued to shrink and approached the hardness profile obtained in this study.

Consistent with an earlier proposition[37] about the decrease in the hardness of the HPT processed sample due to recrystallization of regions in the peripheral regions (i.e., high strain regions), this study also shows an increase in the grain size in the peripheral region as compared with the central region (as shown in Figure 6). Since such a drastic change in the grain size and thus hardness in the peripheral region were observed in the CP Cu disks processed by HPT only through ½ turn, heterogeneity in the microstructure, which is likely to occur more at relatively small strains, must have made the sample more susceptible for nucleation and growth of the recrystallized grains during ambient-ageing. Overall, the hardness behavior of the central region in the disk after ½ turn is unique, and a detailed investigation on effects of the natural ageing is warranted to fully understand this behavior. It should be noted that the hardness profile of the samples processed by HPT for 10 and 50 turns followed by ambient ageing did not show any abrupt variation in both the microstructure and (hence) the hardness value, which were >3 times higher than the annealed coarse-grained sample without HPT. This retention of the exceptionally high hardness of CP Cu over long periods confirms the potential of the HPT processed samples to be used in long-term applications.

4.2. Structure–Property Relationship for Electrical Conductivity

Electrical resistivity in this study was measured using ≈1 mm long stripes, which captured the effect of HPT strain on the local electrical conductivity more accurately, as compared with the earlier studies using much longer samples. Figure 4 shows that HPT processing following by ambient ageing increased the resistivity of CP Cu by only ≈20 % at the strains where it enhanced the hardness by ≈300%. As a matter of fact, the electrical resistivity of the CP Cu samples was significantly smaller than those reported on the HPT-processed CP Cu[19,20] and was in the range of those reported for the HPT-processed high-purity Cu samples. Perhaps, such a combination of high conductivity and excellent hardness has never been reported in CP Cu,

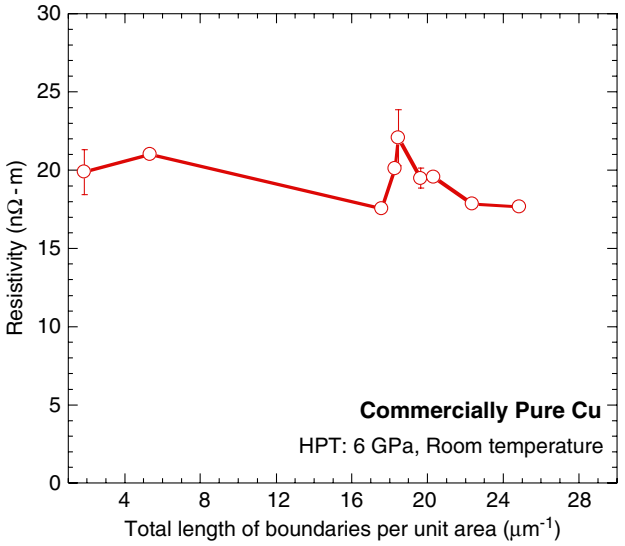

Figure 11. Variation of the electrical resistivity of CP–Cu samples processed through HPT followed by ambient-ageing for 21 months as function of the total length per unit area of grain boundaries.

and the HPT-processed CP Cu has an excellent potential for the electrical connector applications.

To understand the role of the total length of grain boundaries in the electrical conductivity of the HPT-processed CP Cu, variation of the electrical resistivity was plotted with the total length per unit area of the grain boundaries, and the plot is shown in **Figure 11**. It should be noted that since the l_{TGB} was not available at every location or strain at which the electrical resistance values were measured, its value for a given location or strain was interpolated from the two nearest values. Also, since the lengths of twin boundaries were much smaller than those of grain boundaries, its contribution to the total electrical resistivity was assumed to be not significant. As shown in Figure 11, the electrical resistivity of the HPT-processed CP Cu samples varied nonmonotonically with l_{TGB}, thereby suggesting that grain boundaries did not play a significant role in electron scattering and hence determining the electrical conductivity of these samples. It implies that some other phenomenon, such as electron–phonon scattering as suggested by Zhilyaev et al.,[19] is responsible for the observed effect of strain imposed by HPT on the electrical conductivity. Nevertheless, since two independent phenomena control the effect of HPT processing on the hardness and the electrical conductivity, it is possible to enhance both of them at the same time. The present study demonstrated that HPT processing to large numbers of turns followed by ambient-ageing is conducive in obtaining an excellent combination of reasonable electrical conductivity and excellent hardness in the CP Cu. Further experiments are necessary to understand the details of the parameters for controlling the electronic conductivity in the HPT-processed materials.

5. Summary and Conclusions

1) Grain size of the CP Cu samples decreased with HPT processing, except in the regions away from the center of the disks processed through ½ turn of HPT. The saturated grain size of ≈300 nm was achieved after HPT straining of ≈40. The low-strained sample, e.g., after ½ turn, involved large numbers of twin boundaries, whose fraction decreased with continued HPT processing. The length of high angle grain boundaries also increased with strain imposed during HPT processing.

Hardness of the CP Cu samples increased upon HPT processing and the hardness profile across the disk became uniform after 10 turns by HPT. After 50 turns of HPT, the hardness increased to a maximum value of ≈160 HV. On the contrary, the hardness profile of the CP Cu disk after HPT ½ turn showed an evolution in hardness with microstructural recovery and recrystallization, such that high hardness was observed in the central region, whereas the peripheral region showed low hardness.

The electrical resistivity of the CP Cu samples varied nonmonotonically with a total variation of ±10% after HPT straining followed by ambient-ageing. However, it did not show a monotonous variation with the total length of all types of grain boundaries.

Acknowledgements

This study was supported in part by Ministry of Human Resource Development, Government of India (A.R., S.P.S., and P.K.), and the National Science Foundation of the United States under Grant No. DMR-1810343 (M.K. and J.K.H.).

Conflict of Interest

The authors declare no conflict of interest.

Keywords

ambient ageing, hardness, high-pressure torsion, resistivity, ultrafine-grained materials

Received: May 12, 2019
Revised: July 3, 2019
Published online: August 8, 2019

[1] R. Z. Valiev, Y. Estrin, Z. Horita, T. G. Langdon, M. J. Zehetbauer, Y. T. Zhu, *JOM* **2000**, *58*, 33.
[2] R. Z. Valiev, Y. Estrin, Z. Horita, T. G. Langdon, M. J. Zehetbauer, Y. T. Zhu, *JOM* **2016**, *68*, 1216.
[3] R. Z. Valiev, Y. Estrin, Z. Horita, T. G. Langdon, M. J. Zehetbauer, Y. T. Zhu, *Mater. Res. Lett.* **2016**, *4*, 1.
[4] T. G. Langdon, *Acta Mater.* **2013**, *61*, 7035.
[5] R. Z. Valiev, T. G. Langdon, *Prog. Mater. Sci.* **2006**, *51*, 881.
[6] A. P. Zhilyaev, T. G. Langdon, *Prog. Mater. Sci.* **2008**, *53*, 893.
[7] A. P. Zhilyaev, S. Lee, G. V. Nurislamova, R. Z. Valiev, T. G. Langdon, *Scr. Mater.* **2001**, *44*, 2753.
[8] A. P. Zhilyaev, G. V. Nurislamova, B. K. Kim, M. D. Baró, J. A. Szpunar, T. G. Langdon, *Acta Mater.* **2003**, *51*, 753.
[9] M. Kawasaki, *J. Mater. Sci.* **2014**, *49*, 18.
[10] M. Kawasaki, R. B. Figueiredo, Y. Huang, T. G. Langdon, *J. Mater. Sci.* **2014**, *49*, 6586.
[11] F. Wetscher, R. Pippan, *Philos. Mag.* **2006**, *86*, 5867.
[12] G. Khatibi, J. Horky, B. Weiss, M. J. Zehetbauer, *Int. J. Fatigue* **2010**, *32*, 269.

[13] A Hohenwarter, R Pippan, *Philos. Trans. R. Soc.* **2015**, *A373*, 20140366.
[14] N. Gao, C. T. Wang, R. J. K. Wood, T. G. Langdon, *J. Mater. Sci.* **2012**, *47*, 4779.
[15] K. Edalati, M. Ashida, Z. Horita, T. Matsui, H. Kato, *Wear* **2014**, *310*, 83.
[16] E. Aal, M. I. Abd, H. S. Kim, *Mater. Design* **2014**, *53*, 373.
[17] J.-K. Han, H.-J. Lee, J.-I. Jang, M. Kawasaki, T. G. Langdon, *Mater. Sci. Eng.* **2017**, *A684*, 318.
[18] K. Edalati, K. Imamura, T. Kiss, Z. Horita, *Mater. Trans.* **2012**, *53*, 123.
[19] A. P. Zhilyaev, I. Shakhova, A. Belyakov, R. Kaibyshev, T. G. Langdon, *J. Mater. Sci.* **2014**, *49*, 2270.
[20] A. P. Zhilyaev, I. Shakhova, A. Belyakov, R. Kaibyshev, T. G. Langdon, *Wear* **2013**, *305*, 89.
[21] R. K. Islamgaliev, K. M. Nesterov, Y. Champion, R. Z. Valiev, *IOP Conf. Ser.: Mater. Sci. Eng.* **2014**, *63*, 012118.
[22] S. V. Dobatkin, J. Gubicza, D. V. Shangina, N. R. Bochvar, N. Y. Tabachkova, *Mater. Lett.* **2015**, *153*, 5.
[23] E. O. Hall, *Proc. Phys. Soc., London, Sect. B* **1951**, *64*, 747.
[24] N. J. Petch, *J. Iron Steel Inst.* **1953**, *174*, 25.
[25] E. Schafler, G. Steiner, E. Korznikova, M. Kerber, M. J. Zehetbauer. *Mater. Sci. Eng.* **2015**, *A410–411*, 169.
[26] T. Mungole, N. Nadammal, K. Dawra, P. Kumar, M. Kawasaki, T. G. Langdon, *J. Mater. Sci.* **2013**, *48*, 4671.
[27] R. C. Weast, *CRC Handbook of Chemistry and Physics*, 64th ed., CRC Press, Boca Raton **1984**.
[28] http://www.substech.com/dokuwiki/doku.php?id=commercially_pure_nickel_270_high_purity_nickel (accessed: May 2019).
[29] https://e-shop.struers.com/US/EN/documents/40900032_Msds_US_English_3deb2839a3f62f75ed5e73f3b2e84b80.aspx (accessed: May 2019).
[30] P. Kumar, M. Kawasaki, T. G. Langdon, *J. Mater. Sci.* **2016**, *51*, 7.
[31] K. Edalati, Z. Horita, *Mater. Trans.* **2010**, *51*, 1051.
[32] K. Edalati, Z. Horita, *Mater. Sci. Eng.* **2011**, *A528*, 7514.
[33] Y. Huang, S. Sabbaghianrad, A. I. Almazrouee, K. J. Al-Fadhalah, S. N. Alhajeri, T. G. Langdon. *Mater. Sci. Eng.* **2016**, *A656*, 55.
[34] A. I. Almazrouee, K. J. Al-Fadhalah, S. N. Alhajeri, Y. Huang, T. G. Langdon, *Adv. Eng. Mater.* **2019**, *21*, 1801300.
[35] K. Lu, L. Lu, S. Suresh, *Science* **2009**, *324*, 349.
[36] K. Edalati, Y. Ito, K. Suehiro, Z. Horita, *Int. J. Mater. Res.* **2009**, *100*,1668.
[37] Y. Huang, S. Sabbaghianrad, A. I. Almazrouee, K. J. Al-Fadhalah, S. N. Alhajeri, N. X. Zhang, T. G. Langdon, *J. Mater. Res. Tech.* **2017**, *6*, 390.